Global relativistic folding optical potential and the relativistic Green's function model

M. V. Ivanov
Grupo de Física Nuclear, Departamento de Física Atómica, Molecular y Nuclear, Universidad Complutense de Madrid, CEI Moncloa, 28040 Madrid, Spain
and Institute for Nuclear Research and Nuclear Energy, Bulgarian Academy of Sciences, Sofia 1784, Bulgaria

J. R. Vignote
Grupo de Física Nuclear, Departamento de Física Atómica, Molecular y Nuclear, Universidad Complutense de Madrid, CEI Moncloa, 28040 Madrid, Spain

R. Álvarez-Rodríguez
Departamento de Estructura y Física de la Edificación, ETS Arquitectura, Universidad Politécnica de Madrid, E-28040 Madrid, Spain

A. Meucci and C. Giusti
Dipartimento di Fisica, Università degli Studi di Pavia and INFN, Sezione di Pavia, via Agostino Bassi 6, I-27100 Pavia, Italy

J. M. Udías
Grupo de Física Nuclear, Departamento de Física Atómica, Molecular y Nuclear, Universidad Complutense de Madrid, CEI Moncloa, 28040 Madrid, Spain

(Received 18 May 2015; revised manuscript received 30 May 2016; published 14 July 2016)

Optical potentials provide critical input for calculations on a wide variety of nuclear reactions, in particular, for neutrino-nucleus reactions, which are of great interest in the light of the new neutrino oscillation experiments. We present the global relativistic folding optical potential (GRFOP) fits to elastic proton scattering data from ^{12}C nucleus at energies between 20 and 1040 MeV. We estimate observables, such as the differential cross section, the analyzing power, and the spin rotation parameter, in elastic proton scattering within the relativistic impulse approximation. The new GRFOP potential is employed within the relativistic Green's function model for inclusive quasielastic electron scattering and for (anti)neutrino-nucleus scattering at MiniBooNE kinematics.

DOI: 10.1103/PhysRevC.94.014608

I. INTRODUCTION

In recent years joint experimental efforts have been carried out all over the world to detect and study neutrino interactions with the goal to gather information on the necessary extensions of the standard model [1–4]. With weakly interacting probes, dense nuclear targets are needed and the interpretation of the experimental data in terms of neutrino properties requires proper control of neutrino-nucleus interactions. The treatment of nuclear effects represents one of the main sources of systematic uncertainty in the experimental determination of neutrino oscillation parameters.

Recently, the MiniBooNE Collaboration has produced high-quality data, using a mostly carbon target, for a number of selected channels, in particular, for the quasielastic (QE) one, that is, where no pions are detected in the final state. In the QE kinematic region, where the nuclear response to an electroweak probe is dominated by single-nucleon scattering with direct one-nucleon emission, a proper description of the final state interactions (FSIs) of the ejected nucleon with the residual nucleus is very important for the comparison with data. This is a very complex many-body process that one can only hope to model approximately. Different approaches have been developed to describe FSIs. In particular, the relativistic Green's function (RGF) model has been quite successful in the description of data for QE electron and neutrino-nucleus scattering. The model was originally developed within a nonrelativistic framework [5,6] and then within a relativistic framework [7,8] for the inclusive QE electron scattering, it was successfully applied to electron scattering data [5–7,9–11], and it was later extended to neutrino-nucleus scattering [12–20]. The RGF model provides a satisfactory description of the charged-current QE (CCQE) MiniBooNE and MINERνA data, both for neutrino and antineutrino scattering, and of the neutral-current elastic (NCE) MiniBooNE data without the need to increase the standard value of the axial mass. The RGF model can be employed to model FSIs in inclusive processes from the complex optical potential (OP) derived from elastic proton-nucleus scattering data. The RGF formalism can translate the flux lost toward inelastic channels, represented in the imaginary part of the OP, into the right strength observed in inclusive reactions.

The RGF model thus becomes a powerful tool to include in a less model-dependent way the inelastic contributions that are not included in other models based on the impulse approximation (IA) that have been developed to describe FSIs in QE lepton-nucleus scattering. Indeed, one of the most appealing features of the RGF formalism is that, provided a detailed account of the contributions of each possible channel is not needed by the experiment, as it is the case of inclusive electron-nucleus or neutrino-nucleus scattering, these inelastic channels are not included explicitly in RGF calculations, but

they can rather be incorporated from the OP that can be extracted directly from the phenomenology of elastic nucleon-nucleus scattering data. The RGF then bears the potential to produce accurate model-independent predictions of inclusive observables.

There are, however, some important caveats. The RGF needs the optical potential to be given in a large range of energies for the outgoing nucleus, and, further, the situation is such that the available data will not completely constrain the shape and the size of the optical potentials. The RGF has been tested, in particular, with the series of global (i.e., spanning a large range of kinetic energies of the nucleon) energy-dependent (ED) optical potentials from Cooper *et al.* [21,22], in the A-independent (EDAI) and A-dependent (EDAD) versions. These potentials represent, so far, the main, if not the only, successful available global relativistic OPs. Such global potentials are fully phenomenological; just fitted to data assuming smooth and reasonable shapes for the different ingredients (volume and surface terms), they describe elastic proton-nucleus scattering observables at a similar good level, but they exhibit rather different sizes and shapes, at times even rather odd shapes, of the imaginary part. As said, elastic observables constrain the OP only to a certain extent and, in particular, the imaginary part derived from fits to data may be very sensitive to small details of the way the fit to data is performed [23]. The different imaginary parts do not affect significantly elastic observables, but they mean different inelastic contributions and, therefore, sizable differences and theoretical uncertainties when these different OPs are employed to compute RGF predictions.

To reduce the theoretical uncertainties and to ascertain to what extent the RGF predictions can be relied upon, the need arises to build additional global OPs, preferably in a relativistic form, in the largest possible energy range and, whenever possible, with a less phenomenological embodiment. This is the motivation of the present work. We note that the OP is a crucial and critical input not only for RGF calculations but also for the exclusive $(e,e'p)$ reaction and for a variety of other nuclear reactions. Then, as an alternative to the use of purely phenomenological shapes, in this work we chose to build OPs from a folding approach. In this way the shape of the potential is severely dictated by the assumed shape of the nuclear density, while the strength of the different contributions, in particular, the real and imaginary parts, will essentially be dictated by their respective contents in the effective parametrization of the nucleon-nucleon (NN) scattering amplitudes.

Indeed, within the "relativistic impulse approximation" (RIA) one can build OPs to study nucleon-nucleus reactions which provide excellent quantitative descriptions of complete sets of elastic proton scattering observables from various spin-saturated spherical nuclei [24,25]. The validity of the RIA has been demonstrated by the fact that, for energies between 200 and 400 MeV [24,25], these OPs give elastic proton scattering observables very similar to the corresponding ones obtained with the successful global phenomenological OPs [22,26], which, as mentioned before, have been calibrated to provide excellent quantitative decriptions of elastic proton scattering data from stable nuclei, ranging from ^{4}He to ^{208}Pb, and for incident energies between 20 and 1040 MeV.

The relativistic Horowitz-Love-Franey (HLF) model parametrizes the NN scattering amplitudes as a number of Yukawa-type meson-exchange terms. In the original HLF model [24,25] pp and pn scattering amplitudes at discrete incident energies of 135, 200, and 400 MeV are parametrized. Maxwell has developed energy-dependent parametrizations of the NN scattering amplitudes for two energy ranges, namely, 200–500 MeV [27] and 500–800 MeV [28]. Li *et al.* [29,30] have generated an energy-dependent Lorentz covariant parametrization of the on-shell NN scattering amplitudes for laboratory kinetic energies between 50 and 200 MeV. At these low energies, multiple scattering effects [31], medium modifications of the NN interaction [32], and Pauli blocking [25,33] contributions are important. Li *et al.* [29] have established that phenomenological Pauli blocking effects and density-dependent corrections to the σN and ωN meson-nucleon coupling constants modifying the RIA microscopic scalar and vector optical potentials make it possible to obtain a consistent and quantitative description of all elastic scattering observables (the differential cross section $d\sigma/d\Omega$, the analyzing power A_y, and the spin rotation parameter Q) at energies ranging from as low as 30 and up to 200 MeV. Beyond that energy value, medium effects were considered less important. However, Sakaguchi *et al.* [34] have shown that medium modifications of the NN interaction are important not only at low energies. The authors managed to explain their experimental data (elastic proton scattering from ^{58}Ni at $E_p = 192$, 295, and 400 MeV) at backward angles within the framework of the RIA by using experimental densities deduced from electron scattering and by modifying the coupling constants and the masses of the exchanged mesons in the NN interaction. It is interesting to note that Sakaguchi *et al.* [34] have compared the experimental data with three models: the original HLF model; the RIA (IA2) by Tjon and Wallace [35–37], which is based on the general representation of the NN scattering amplitudes in the full Dirac space; and the folding model using a nonrelativistic G matrix proposed by the Hamburg group [38,39]. None of the three models can satisfactorily explain the experimental data. After calibration of the effective NN interaction in Ref. [34] for the ^{58}Ni nucleus, Zenihiro *et al.* [40] and Terashima *et al.* [41] have deduced the neutron density distributions of Pb and Sn isotopes, respectively, in the form of a model-independent sum-of-Gaussians distribution. The Melbourne group has developed a highly predictive microscopic Schrödinger model for describing elastic scattering at energies between 20 and 800 MeV [32,42,43], where the complex OPs were formed by folding effective NN interactions with the density matrices of the nuclear ground state.

Microscopical optical potentials can be obtained by folding realistic nuclear densities with an effective nuclear interaction fitted only to NN phase shifts [32,38,39,42–46] and also within the framework of the Dirac-Brueckner-Hartree-Fock approach [47]. These OPs are in general able to give a good description of elastic proton-nucleus scattering data, although not as good as with purely phenomenological OPs, which, on the other hand, suffer from ambiguities in the interpretation of the parameters, since different parametrizations, that is different optical potentials, may fit the data equally well.

The focal point of the present work is the RGF approach to inclusive lepton-nucleus scattering, aiming to reproduce quasielastic neutrino scattering data from MiniBooNE. Many efforts, both from the experimental and the theoretical side, have been devoted to understanding those data. Usual models based on the IA generally underpredict the MiniBooNE data. A good description of data is given by models with increased 2p-2h meson-exchange currents due to tensor correlations [48–54] and by RGF calculations, where pure mean-field correlations and no explicit 2p-2h contributions are included, meson-exchange currents are neglected, and FSIs are taken into account using purely phenomenological OPs. The RGF results are, however, sensitive to the parametrization adopted for the phenomenological optical potential. In particular, different parametrizations give very large differences in the total CCQE cross section [12], which is described using only one (EDAI) of the available global phenomenological relativistic OPs. It seemed therefore of immediate interest to analyze this result in depth, because good modelization and understanding of the nuclear interactions of the neutrino target employed in this experiment is a necessary input which is being pursued by a large part of the experimental neutrino community. To this aim, it is important to assess the RGF response with a larger variety of OPs and, in particular, with a potential derived with a very different methodology than the global parametrizations of Cooper *et al.* [21,22], if possible with more constrained geometries. Relativistic folding potentials are essentially constrained to follow the shape of the nuclear density, thus the geometries are well controlled and they have been employed successfully to describe elastic proton scattering. Because good agreement with elastic scattering data is considered of paramount importance, we tune the effective interaction to fit the available elastic proton scattering from carbon; thus in this way medium effects will be taken into account.

In this work a new microscopic global relativistic folding optical potential is generated by folding the HLF t matrix with the relevant relativistic mean-field Lorentz densities via the so-called $t\rho$ approximation. Two basic ingredients underlie the realization of these folding potentials, namely, a suitable analytical representation for the *NN* interaction and an appropriate relativistic model of nuclear densities. We have derived an energy-dependent parametrization of the on-shell *NN* scattering matrix at incident laboratory kinetic energies ranging from 20 to 1040 MeV for the ^{12}C nucleus. In comparison with the phenomenological EDAI potentials of Refs. [22,26], the following are true of the folding potential obtained in our analysis:

(i) It is derived from all available experimental data on proton elastic scattering that we are aware of.
(ii) It stems from a folding approach, with neutron density fitted to data and proton density taken from electron scattering experiments.
(iii) The same nuclear densities are used at all the energies from 20 to 1040 MeV.
(iv) The imaginary term of the optical potential is built from the effective *NN* interaction.

The paper is organized as follows. In Sec. II we outline the general formalism used in our calculations: we present briefly the method that has been used to obtain our new microscopic global relativistic folding optical potential (GRFOP) and give its main properties, and we discuss the main features of the RGF model. Section III contains the RGF results for the inclusive QE electron scattering and for (anti)neutrino CCQE and NCE cross sections at MiniBooNE kinematics. We show a detailed analysis of the sensitivity to the choice of the OP and compare the RGF results obtained with the new GRFOP and with the previous phenomenological EDAI and EDAD1 potentials. Finally, in Sec. IV we summarize our results and present our concluding remarks.

II. FORMALISM

A. Global relativistic folding optical potential (GRFOP)

We focus on the ^{12}C nucleus, which is often used in neutrino-nucleus experiments, especially in the light of recently published (anti)neutrino CCQE and NCE experimental data [55–58]. The method is based on the framework of the RIA using the relativistic HLF model [24,25,59], where the nucleon-nucleus optical potential is calculated by folding the Love-Franey *NN* interaction with the nucleon vector and scalar density of the target nucleus. Originally, in the HLF approach, density distributions (vector and scalar densities for protons and neutrons) were calculated using, for instance, the relativistic Hartree (RH) calculation code TIMORA introduced by Horowitz and Serot [60]. It is shown in Ref. [34], and it is confirmed by our present analysis, that a RH density distribution has difficulties in reproducing in detail the behavior of scattering observables, even if some parameters of the effective *NN* interaction are fitted to nucleon-nucleus scattering data. In our calculations we obtain the vector proton density distribution from the charge distribution measured by electron scattering, unfolding the free proton charge form factor from the experimental charge distribution taken as the sum of Gaussians [61]:

$$\rho_V^p(r) = \frac{1}{(2\pi)^3}\int d^3q e^{-i\vec{q}\cdot\vec{r}}\tilde{\rho}_V^p(q), \tag{1}$$

where

$$\tilde{\rho}_V^p(q) = \frac{\int d^3q e^{i\vec{q}\cdot\vec{r}}\rho_c(r)}{G(q)}. \tag{2}$$

Here $\rho_c(r)$ is the experimental charge density and $G(q)$ is the proton form factor. The point proton density $\rho_V^p(r)$ is normalized to the number of protons Z and the neutron density $\rho_V^n(r)$ is normalized to the number of neutrons N. This procedure yields the vector densities. Our study of different procedures to find the scalar density shows that in the case of spherical nuclei [62] the following relation between scalar and vector densities,

$$\frac{\rho_S(r)}{\rho_V(r)} \simeq \text{const.}, \tag{3}$$

gives, in comparison with other procedures, better results for the scattering observables derived from folding potentials. Thus, scalar densities are assumed to be proportional to the vector ones, and the proportionality constant can be calculated from the relation between vector and scalar densities

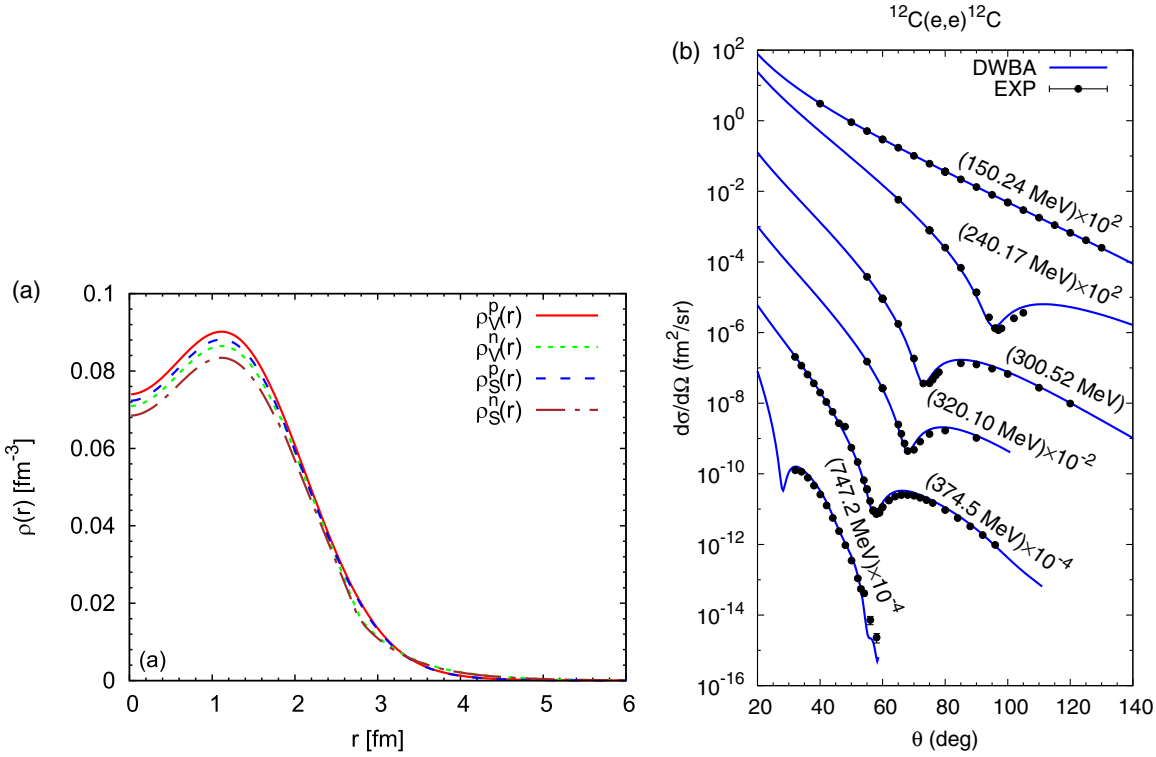

FIG. 1. (a) The proton and neutron scalar and vector densities obtained and used in our analysis. (b) The elastic electron scattering cross sections from ^{12}C in DWBA. The experimental data are from Refs. [76,77].

obtained in the relativistic mean-field (RMF) theory with NLSH parameters [63,64], and the constant of Eq. (3) is determined by

$$\text{const.} = \frac{4\pi \int \rho_S^{\text{NLSH}}(r) r^2 dr}{4\pi \int \rho_V^{\text{NLSH}}(r) r^2 dr}. \tag{4}$$

Using Eq. (4) and the RMF theory with NLSH parameters, we have found for ^{12}C the scalar/vector ratio: for protons $\rho_S^p(r)/\rho_V^p(r) = 0.969$ and for neutrons $\rho_S^n(r)/\rho_V^n(r) = 0.968$. In Ref. [65] (Chap. 4, Fig. 4.16) Terashima has shown a weak mass-number (A) dependence of the ratios on the integrated scalar and vector densities, which is less than 1% for $A \geqslant 16$.

The data used in our analysis (proton elastic scattering differential cross sections and analyzing powers) are in the range 20 to 1040 MeV. Specifically, we consider the data taken at 21.1 and 79.8 [66], 122.0 [67], 160.0 [67], 200 [68], 250 [69], 300 [70], 398 [71], 494 [72], 597, 698 [71], 800 [73,74], and 1040 [75] MeV. We restrict to scattering angles smaller than 90°, or angles corresponding to momentum transfers below 3 fm^{-1}, whichever is smaller, similarly to Ref. [26]. In the fitting procedure we use a definition of χ^2 similar to the one given in Ref. [22]:

$$\begin{aligned} \chi^2 &= \chi^2_\sigma + \chi^2_{A_y}, \\ \chi^2_\sigma &= \frac{1}{N_\sigma} \sum_{i=1}^{N_\sigma} \left[\frac{F_N \sigma^{\text{exp}}(i) - \sigma^{\text{theo}}(i)}{\Delta\sigma(i)} \right]^2, \\ \chi^2_{A_y} &= \frac{1}{N_{A_y}} \sum_{i=1}^{N_{A_y}} \left[\frac{A_y^{\text{exp}}(i) - A_y^{\text{theo}}(i)}{\Delta A_y(i)} \right]^2, \end{aligned} \tag{5}$$

where F_N is the normalization of the cross-section data,

$$F_N = \frac{\sum_{i=1}^{N_\sigma} \{\sigma^{\text{exp}}(i)\sigma^{\text{theo}}(i)/[\Delta\sigma(i)]^2\}}{\sum_{i=1}^{N_\sigma} \{[\sigma^{\text{exp}}(i)]^2/[\Delta\sigma(i)]^2\}}, \tag{6}$$

and N_σ and N_{A_y} are the numbers of cross sections and analyzing power points, respectively, in the data set.

To determine the neutron densities, first we have compared three on-shell NN parametrizations at 200 MeV, namely, Li *et al.* [29,30], Maxwell [27], and the original HLF model [24,25], assuming $\rho_V^n(r) = \rho_V^p(r)$. Using the proton and neutron densities and all the already mentioned available NN parametrizations [24,25,27,29,30], we compared which one gives the best χ^2 results against the proton scattering data at a proton energy of 200 MeV, where all parametrizations have parameters, that is, where all of them overlap. The best results were obtained using the Li *et al.* parametrization [29,30]. Thus we use as input the Li *et al.* parametrization at 200 MeV and the proton density from the experimental charge distribution and start a fitting procedure of the neutron density to the data at 200 MeV. In this fit we just tune the neutron radius by a few percent, until the best agreement is obtained. This concludes our procedure to determine the neutron density.

The neutron vector and scalar densities obtained with this procedure are shown in Fig. 1(a), along with the proton densities taken from the assumed experimental charge distribution, unfolded by the proton form factor. We then test these proton and neutron (which yields a small contribution to the charge density) vector densities, building from them the charge density of the ^{12}C nucleus and calculating the elastic electron scattering cross sections within the distorted-wave

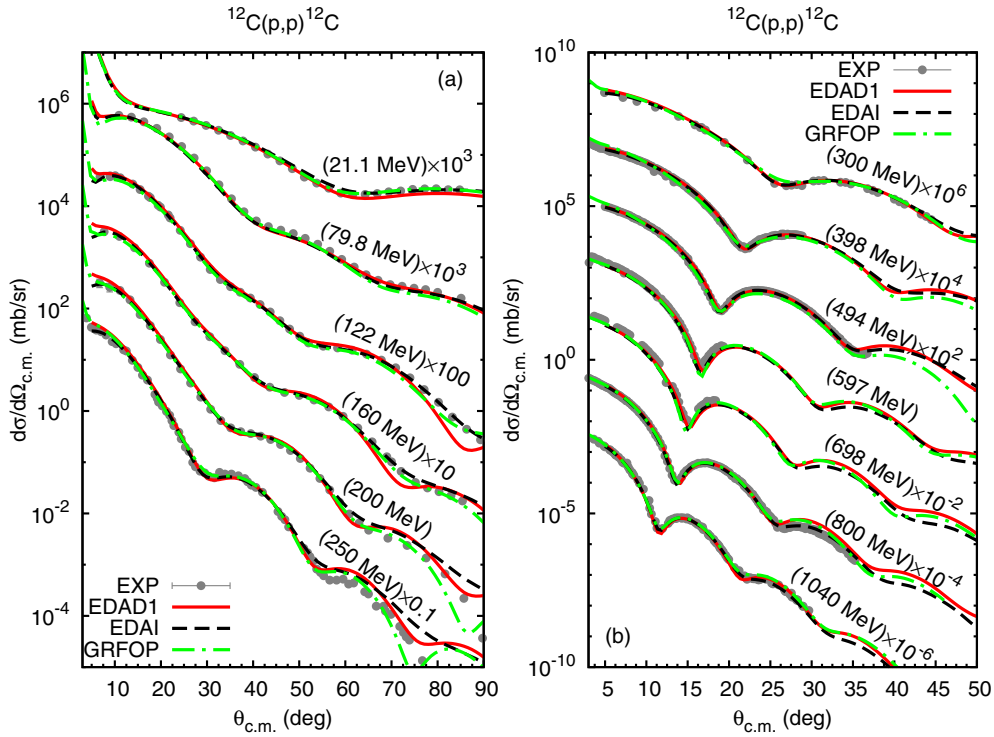

FIG. 2. Differential cross section for the elastic scattering of protons with $T_p = 20$–1040 MeV from ^{12}C. The dash-dotted curves display our predictions obtained using the GRFOP. The results obtained with EDAI (dashed line) and EDAD1 (solid line) are also shown for a comparison.

Born approximation (DWBA). In Fig. 1(b) we compare our DWBA results with the available experimental data of Refs. [76,77]. It can be seen that our results are in very good agreement with the experimental data.

After we have fixed the proton and neutron densities of the ^{12}C nucleus, and in order to extend the approach down to 20 MeV and up to 1040 MeV, we have followed the procedure to incorporate medium effects in the new OP that we call the GRFOP. We have used the following fitting procedure of *NN* parameters at different energies (for which exist experimental data). As a starting point, for the energy range 20–500 MeV, we used the Li *et al.* [29,30] parametrization at 200 MeV. In the range between 20 and 200 MeV, where there is the largest number of experimental data, we used more intermediate energy points in the fitting procedure. Above 200 MeV, where fewer experimental data sets are available, we used, for several energies, the scattering observables taken from the EDAI potential. We fitted the parameters of the real and imaginary parts of the coupling constants and the cutoff parameters of mesons, while the masses of the mesons were fixed to the masses from the Li *et al.* parametrization at 200 MeV. For energies above 500 MeV, where the Li *et al.* parametrization doesn't give good results, we used the Maxwell [28] parametrization at 500 MeV as a starting point for the fit. Also in this region we fitted the same parameters (real and imaginary parts of coupling constants and cutoff parameters of mesons), while the masses of the mesons were fixed to the masses from the Maxwell parametrization at 500 MeV. As a consequence, the parameters of our fit are similar to the ones of Li *et al.* at 200 MeV and of Maxwell at 500 MeV, and for other energies they tend to lie in between the values of these two sets. This fine tuning of the parameters, which leads to the renormalization of certain meson-nucleon coupling constants, has been applied for experimental data of proton elastic scattering from ^{12}C in the proton energy range $T_p = 20$–1040 MeV. We did not use all the experimental data in the fitting procedure (for example, 398, 597, and 698 MeV) so that some data sets can be used to test the potential.

In Fig. 2 the differential cross sections of elastic proton ^{12}C scattering calculated with the GRFOP for proton energies $T_p = 20$–1040 MeV are shown and compared with the data. The energy dependence of the experimental cross sections is reproduced quite well by our results. The associated analyzing powers and spin rotation parameters are displayed in Figs. 3 and 4, respectively. Experimental data are not available for the spin rotation parameter. As can be seen in Fig. 3, the calculated analyzing powers agree well with the data. Some discrepancies are found at 200 and 250 MeV for angles above 60° and 55°, respectively, but these data correspond to momentum transfers larger than 3 fm^{-1} and are not taken into account in the fitting procedure. In Figs. 2–4 the results obtained with the EDAI and EDAD1 optical potentials are also shown for a comparison.

To compare the predictions of the proton elastic scattering observables calculated with the three optical potentials (GRFOP, EDAI, and EDAD1), we define the total χ^2 per degree of freedom:

$$\chi^2_{\rm pdf} = \frac{1}{N - N_p} \sum_{j=1}^{N_S} \left[N_\sigma(j) \chi^2_\sigma(j) + N_{A_y}(j) \chi^2_{A_y}(j) \right], \quad (7)$$

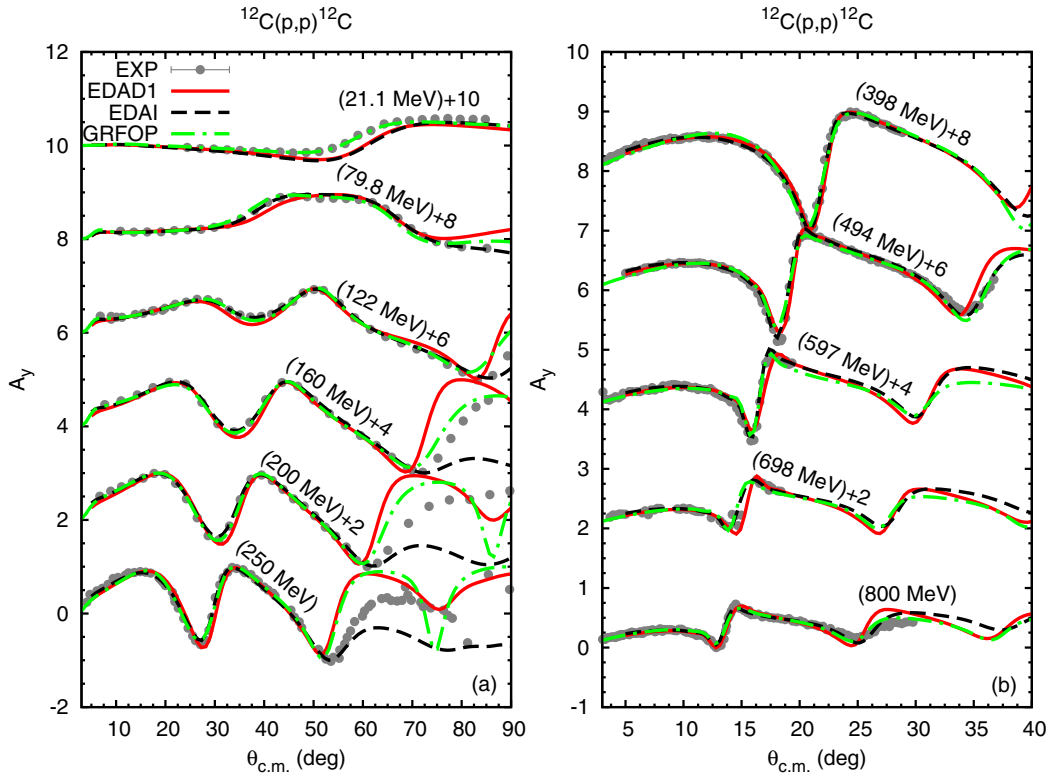

FIG. 3. Analyzing power for the elastic scattering of protons with $T_p = 20$–800 MeV from ^{12}C. Line convention is as in Fig. 2.

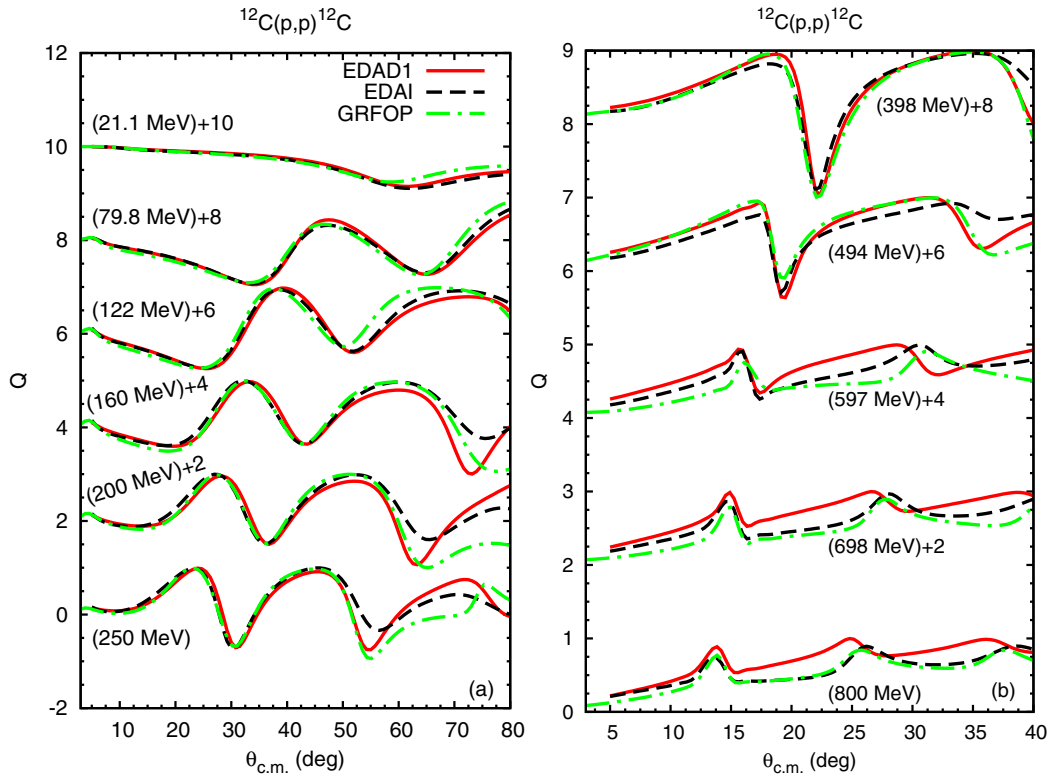

FIG. 4. Spin rotation parameter for the elastic scattering of protons with $T_p = 20$–800 MeV from ^{12}C. Line convention is as in Fig. 2.

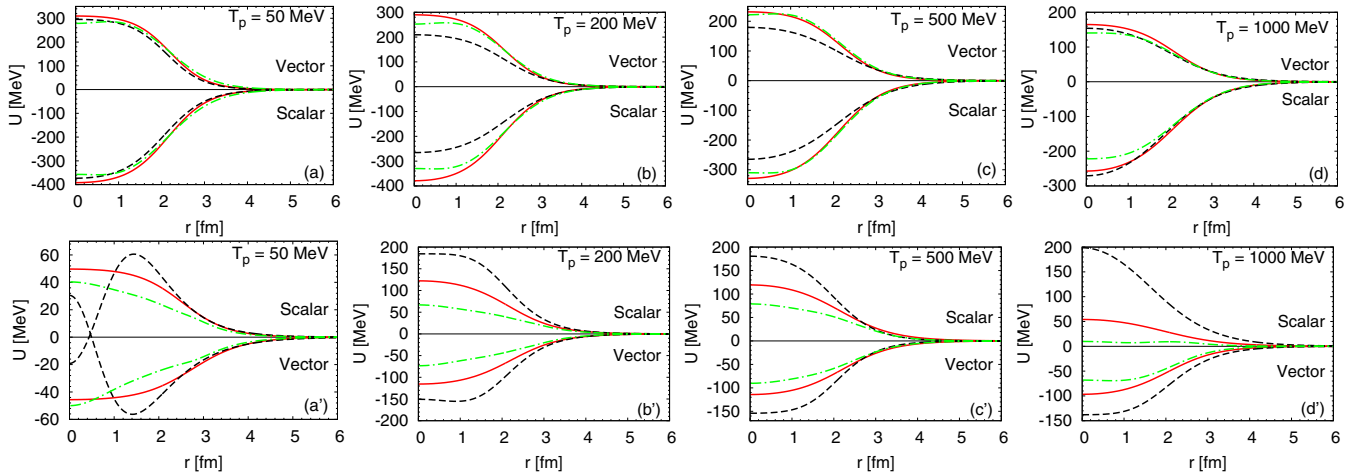

FIG. 5. The real scalar and vector optical potentials for ^{12}C at $T_p = 50$ MeV (a), 200 MeV (b) 500 MeV (c), and 1000 MeV (d): EDAI, dashed lines; EDAD1, solid lines; and GRFOP, dash-dotted lines. The corresponding imaginary parts are shown in panels (a′)–(d′).

where N is the total number of data points, N_p is the number of the parameters, and N_S is the total number of data sets. In this analysis we use all available experimental data of proton elastic scattering [78]. With the above given restrictions, i.e., data sets for angles smaller than 90° or angles corresponding to a momentum transfer below 3 fm^{-1}, the values of $\chi^2_{\rm pdf}$ for the three OPs are as follows:

$$\begin{aligned} \chi^2_{\rm pdf}({\rm EDAI}) &= 2.2, \\ \chi^2_{\rm pdf}({\rm GRFOP}) &= 4.7, \\ \chi^2_{\rm pdf}({\rm EDAD1}) &= 5.6. \end{aligned} \tag{8}$$

The GRFOP gives a value of $\chi^2_{\rm pdf}$ between EDAD1 and EDAI. For completeness, we present in Fig. 5 the real and imaginary scalar and vector parts of the GRFOP, EDAI, and EDAD1 optical potentials calculated for ^{12}C at proton energies $T_p = 50$, 200, 500, and 1000 MeV. As can be seen from Fig. 5, the real part of the GRFOP is close to the EDAD1 one, whereas the imaginary part is, in absolute value, lower than the imaginary parts of the EDAI and EDAD1 potentials. Further, the shape of the GRFOP is very similar to the shape of the EDAD1 potential. This is expected, because the folding potentials should have shapes smoothly following the nuclear densities and thus they lack the complex geometries introduced phenomenologically in the EDAI fits. The complex shape of the EDAI optical potentials seems to be correlated with the larger imaginary parts of these potentials and is absent in EDAD1, which bears a simpler geometry.

B. Green's function model

A reliable description of FSI effects is very important for the comparison with data of QE electron scattering [9,79]. For instance, in the exclusive $(e,e'p)$ reaction the use of a complex OP in the distorted-wave impulse approximation (DWIA) allows one to successfully describe a wide number of experimental data [9,79–85]. The imaginary part of the OP produces an absorption representing the loss of flux seen in the elastic channel. Indeed, in the description of elastic nucleon-nucleus scattering the imaginary part of the OP accounts for the fact that, if other channels are open besides the elastic one, part of the incident flux, which otherwise would be seen in the elastic scattering, is lost in the elastically scattered beam and appears in the inelastic channels which are open. This flux may not contribute to the experimental signal if the experiment is performed under exclusive conditions. Thus, in the exclusive $(e,e'p)$ reaction, where the final nuclear state is completely determined, the experimental signal receives contributions mainly from the process where the knocked-out nucleon scatters elastically with the residual system in the final state. In this case, the full optical potential, tuned to reproduce the elastic nucleon-nucleus cross section, represents a good description of the experimental arrangement. In contrast, for inclusive experiments, where only the final lepton (or just the final nucleon) is detected and the final nuclear state is not uniquely determined, elastic and inelastic channels contribute to the experimental signal, which, therefore, will contain contributions also from the flux lost in the elastic channel toward inelastic channels, to a larger or smaller extent depending on the particular experimental situation. The use of the DWIA with an absorptive complex OP would only estimate the contribution of the elastic final state for the proton and would grossly underestimate the cross section measured in inclusive processes.

Different approaches to describe FSIs have been considered in relativistic calculations of inclusive QE electron- and neutrino-nucleus scattering. In the simplest relativistic plane-wave impulse approximation (RPWIA), all FSIs are simply neglected. In other approaches based on the RDWIA, FSIs are incorporated in the final nucleon state by means of a potential which either retains only the real part of the optical potential (rROP) or is just the same relativistic mean-field potential considered in describing the initial nucleon state (RMF) [86,87].

In the RGF model, FSIs are described in the inclusive scattering by means of the complex relativistic OP determined to reproduce the elastic scattering phenomenology, that is, the same OP used to describe the exclusive scattering, but the

RGF formalism allows one to compute the inclusive scattering observables, providing for a formal mean to recover the flux in all the final-state channels. In the RGF model the components of the nuclear response are written in terms of the single-particle optical model Green's function [5–8,10–14,16,19]; taking advantage of its spectral representation, which is based on a biorthogonal expansion in terms of a non-Hermitian OP $\mathcal{H}$ and of its Hermitian conjugate $\mathcal{H}^\dagger$, it is possible to avoid the explicit calculation of the single-particle Green's function and to obtain the components of the hadron tensor [7,13] in terms of matrix elements of the same type as the RDWIA ones of the exclusive $(e,e'p)$ reaction in Refs. [81,84,85], but which involve eigenfunctions of both $\mathcal{H}$ and $\mathcal{H}^\dagger$, where the imaginary part has an opposite sign and gives in one case a loss and in the other case a gain of strength. The RGF formalism makes it possible to reconstruct the flux lost into nonelastic channels, in the case of the inclusive response, starting from the complex OP which describes elastic nucleon-nucleus scattering data. Moreover, it provides a consistent treatment of the FSIs in the exclusive and in the inclusive scattering, and, because of the analyticity properties of the OP, it fulfills the Coulomb sum rule [5,7,88].

A comparison of the results given by these different descriptions of FSIs has been presented in Ref. [10] for inclusive QE electron scattering and in Ref. [14] for CCQE neutrino scattering. The results of the different models have been compared in Ref. [12] with the CCQE MiniBooNE data and in Ref. [19] with NCE neutrino scattering. The behavior of electron scattering data and their related scaling and superscaling functions are, in general, successfully described by both RMF and RGF models. In the case of neutrinos, the shape of the experimental CCQE cross sections is well reproduced by both models and, in addition, the RGF can reproduce the magnitude when the EDAI parametrization of the relativistic OP is adopted, whereas the RMF generally underpredicts the CCQE MiniBooNE data. Similar results are obtained when the flux-averaged NCE cross sections from MiniBooNE are considered.

In comparison with CCQE and NCE MiniBooNE data the RGF results are usually larger than the results of the RMF and of other models based on the IA. This enhancement can be ascribed to the translation to the inclusive strength of the overall effect of the inelastic channels. Within the RGF, however, only the total inclusive contribution can be estimated, not being possible to disentangle different reaction processes, which makes it difficult to explain in detail the origin of the enhancement. The enhancement is linked to the size of the imaginary term of the OP and can be associated, to some extent, with the use of different phenomenological relativistic OPs, some of which exhibit much larger imaginary terms, thus producing larger predictions for inclusive observables. Significant differences can be obtained when RGF calculations are performed with different parametrizations for the OP. The predictions of the model are therefore affected by uncertainties in the determination of the phenomenological OP, because the size of the imaginary term is to a large extent related to the assumed shape of the potential and to the way of performing the fit.

The microscopic GRFOP potential proposed in this paper has been generated as a less phenomenological alternative to purely phenomenological global optical potentials, to study and hopefully reduce the uncertainties introduced in the RGF results by the choice of the OP. In the next section RGF results obtained with the GRFOP for QE electron and (anti)neutrino scattering on ^{12}C are presented and compared with the results obtained with the EDAI and EDAD1 potentials of Refs. [21,22].

III. RESULTS AND DISCUSSION

In this section the numerical results of our RGF calculations with the GRFOP are presented and compared with the corresponding results obtained with the EDAI and EDAD1 optical potentials of Refs. [21,22]. As a first step, the comparison is performed for the ^{12}C(e,e') cross sections and scaling functions. Then, neutrino and antineutrino scattering off ^{12}C is considered and results for the flux-integrated CCQE and NCE cross sections from MiniBooNE are discussed.

A. Electron scattering

In Fig. 6 the RGF results calculated with the three relativistic OPs are compared with the experimental ^{12}C(e,e') differential cross sections for three different kinematics [89–91]. A recent review of the experimental situation, as well as of different theoretical approaches, can be found in Refs. [92,93]. The differences among the three RGF results are qualitatively similar in Figs. 6(a) and 6(b), where the momentum transfer in the kinematical region of the QE peak is approximately the same, i.e., $q \approx 0.55$ GeV/c: the RGF-EDAI cross section is larger than the RGF-EDAD1 and RGF-GRFOP ones. In Fig. 6(c), where the momentum transfer at the peak is around 800 MeV/c, RGF-EDAD1 gives the largest cross section in the peak region and the RGF-EDAI and RGF-GRFOP results are similar. The experimental cross section in Fig. 6(a) is well described in the peak region by the RGF-EDAD1 and RGF-GRFOP calculations and slightly overpredicted by the RGF-EDAI results, in Fig. 6(b) it is slightly underpredicted by all the calculations, and in Fig. 6(c) the results, in particular, the RGF-GRFOP one, show a satisfactory agreement with the magnitude and the shape of the experimental cross section. The agreement with ^{12}C(e,e') data is generally satisfactory, but we are aware that contributions beyond the QE peak, like meson-exchange currents and Delta effects, that may play a significant role in the analysis of data even at the maximum of the QE peak, are not considered in the RGF calculations. The comparison can therefore give only an indication and cannot be considered as conclusive until the relevance of these contributions is carefully evaluated.

The effects already discussed for the differential cross sections are also present in the scaling functions. An exhaustive analysis of QE (e,e') world data has shown that these data, when plotted against a properly chosen scaling variable Ψ', show a mild dependence on the momentum transfer (scaling of the first kind) and almost no dependence on the nuclear target (scaling of the second kind). These properties are well satisfied in the longitudinal channel, while violations associated with effects beyond the impulse approximation, like inelastic scattering and meson-exchange currents, occur

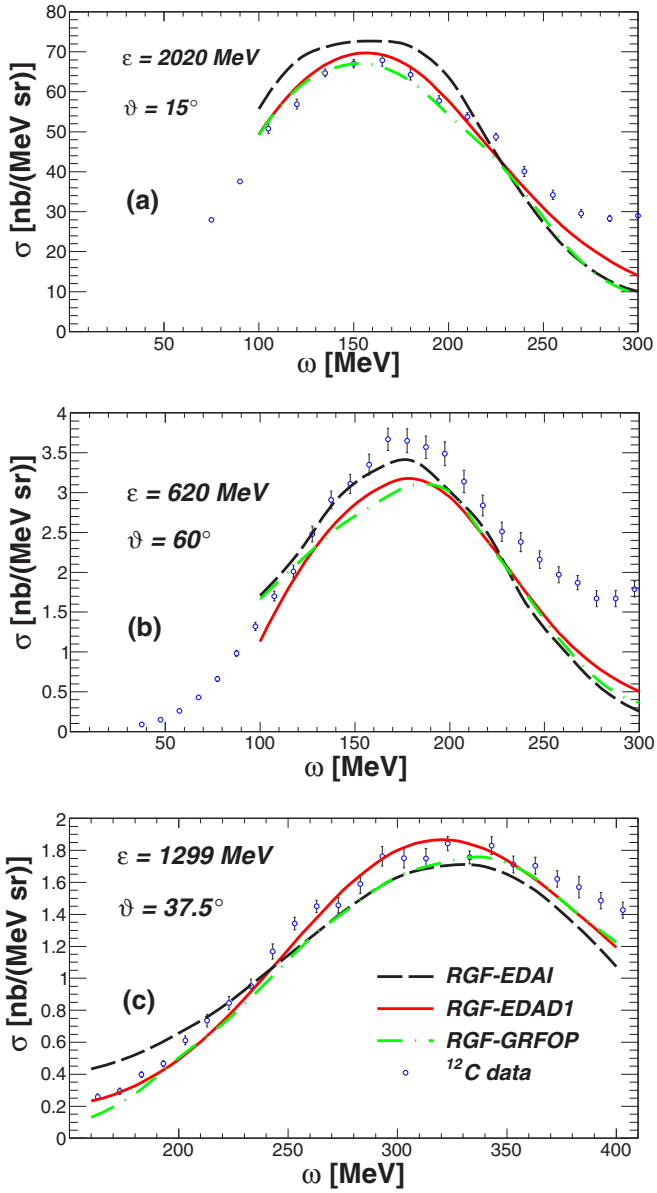

FIG. 6. Differential cross section of the $^{12}C(e,e')$ reaction for different beam energies and electron scattering angles. Experimental data are from Refs. [89–91].

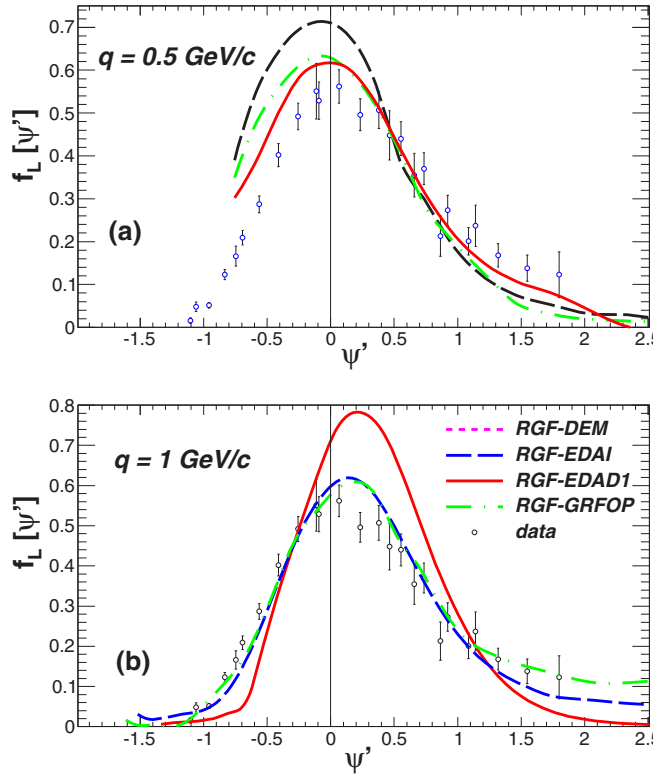

FIG. 7. Longitudinal contributions to the scaling function for $q = 500$ and 1000 MeV/c compared with the averaged experimental scaling function.

mainly in the transverse channel at energies above the QE peak.

The scaling function is usually obtained by dividing the longitudinal contribution to the inclusive differential cross section by the appropriate longitudinal term of the single-nucleon e-N elastic cross section weighted by the corresponding proton and neutron numbers involved in the process (see Refs. [94–97] for details). In Fig. 7 the scaling functions extracted from the longitudinal contribution to the RGF cross sections, calculated for two values of the momentum transfer, are compared with the averaged QE phenomenological scaling function extracted from the analysis of (e,e') world data [94–97]. The most striking feature of the phenomenological function is its asymmetric shape, with a pronounced tail in the region of positive Ψ', that can be reproduced neither within a nonrelativistic approach nor by relativistic models like the relativistic Fermi gas (RFG), the RPWIA, and the rROP. The asymmetric shape is well reproduced by the RMF model [87,98], where FSIs are described by the same strong and real energy-independent mean-field potential that describes the initial nucleon bound state. The RGF model reproduces the asymmetric shape [10]. The different dependence on the momentum transfer shown in Fig. 7 by the three OPs involved in the RGF calculations makes the RGF scaling function tail less pronounced as the value of q goes up. It is interesting to notice the different behavior of the RGF-EDAI and RGF-EDAD1 results in comparison with the phenomenological scaling function: the phenomenological function is reproduced at $q = 0.5$ GeV/c and overestimated at $q = 1$ GeV/c by RGF-EDAD1, while it is overestimated at $q = 0.5$ GeV/c and reproduced at $q = 0.5$ MeV/c by RGF-EDAI. In contrast, the RGF-GRFOP gives only a mild dependence on the momentum transfer and gives a better agreement with the experimental scaling function: one would say that the RGF results with the GRFOP scale better. Actually, this is a very interesting fact. The preservation of scaling, as seen in the data analyzed in the derivation of the universal scaling curve shown in this figure, would certainly dismiss the predictions for the scaling function obtained within the RGF from the two purely phenomenological optical potentials. They simply do not scale enough. The mild departure from scaling shown by the RGF-GRFOP is not only compatible with the data, but actually it is favored, as the actual data exhibit a

slight departure from scaling at a level similar to that of the RGF-GRFOP curve.

B. Neutrino-nucleus scattering at MiniBooNE kinematics

The MiniBooNE Collaboration at FermiLab has recently reported measurements of the neutrino CCQE and neutrino NCE scattering cross sections [56,57] on carbon. In addition, using the same beamline and the same experimental apparatus, the MiniBooNE Collaboration collected a large amount of statistics of data sets in the $\bar{\nu}$ mode and provided the most complete information of the antineutrino CCQE and NCE cross sections [55,58].

Despite many theoretical efforts, the fundamental processes contributing to neutrino interactions with nuclear matter are not well understood. For instance, models based on the IA are generally unable to reproduce the MiniBooNE cross sections [99–102] unless calculations are performed with a value of the axial mass M_A significantly larger ($M_A \sim 1.20$–1.40 GeV/c^2) than the world average value from the deuterium data of $M_A \simeq 1.03$ GeV/c^2 [103,104]. In the models of Refs. [48–54] the contribution of multinucleon excitations to neutrino-nucleus scattering has been found to be sizable and the results agree with the MiniBooNE cross sections, but, on the other hand, a relativistic calculation of 2p-2h excitations, performed for both electron and neutrino scattering [105–108], has shown that two-body currents at MiniBooNE kinematics are unable to fully account for the data. Other models that predict an enhancement of the magnetic response rather than a modification of the axial mass are in agreement with the MiniBooNE data [109,110]. It is therefore evident that a careful evaluation of all nuclear effects, as well as of the relevance of multinucleon emission and of some non-nucleonic contributions [2,3,111–114], is very important for a deeper understanding of the neutrino-nucleus reaction dynamics.

In the analysis of inclusive reactions FSIs are a crucial ingredient for a proper description of the data. The RGF model, where the flux lost to nonelastic channels is recovered through the complex OP, is very interesting because it can provide a satisfactory description of the CCQE MiniBooNE cross sections, for some particular choices of the phenomenological OP, without the need to increase the standard value of the axial mass [12].

In Figs. 8 and 9 the flux-averaged double-differential cross sections per target nucleon for the CCQE neutrino and antineutrino scattering are presented as functions of the muon kinetic energy T_μ for three different bins of the muon scattering angle ϑ_μ. All the calculations are performed adopting the standard value for the axial mass, i.e., $M_A = 1.03$ GeV/c^2. A good agreement with the shape of the experimental cross sections is generally obtained with all the three OPs. The RGF-EDAD1 and RGF-EDAI results are similar in the bin $0.4 \leqslant \cos\vartheta_\mu \leqslant 0.5$. Larger differences, around 20%, are obtained in the peak region for the forward-angle scattering bins, the RGF-EDAI results being larger than the RGF-EDAD1 ones and also in somewhat better agreement with the neutrino scattering data in Fig. 8. In the case of antineutrino scattering of Fig. 9, data are slightly overestimated by the RGF-EDAI

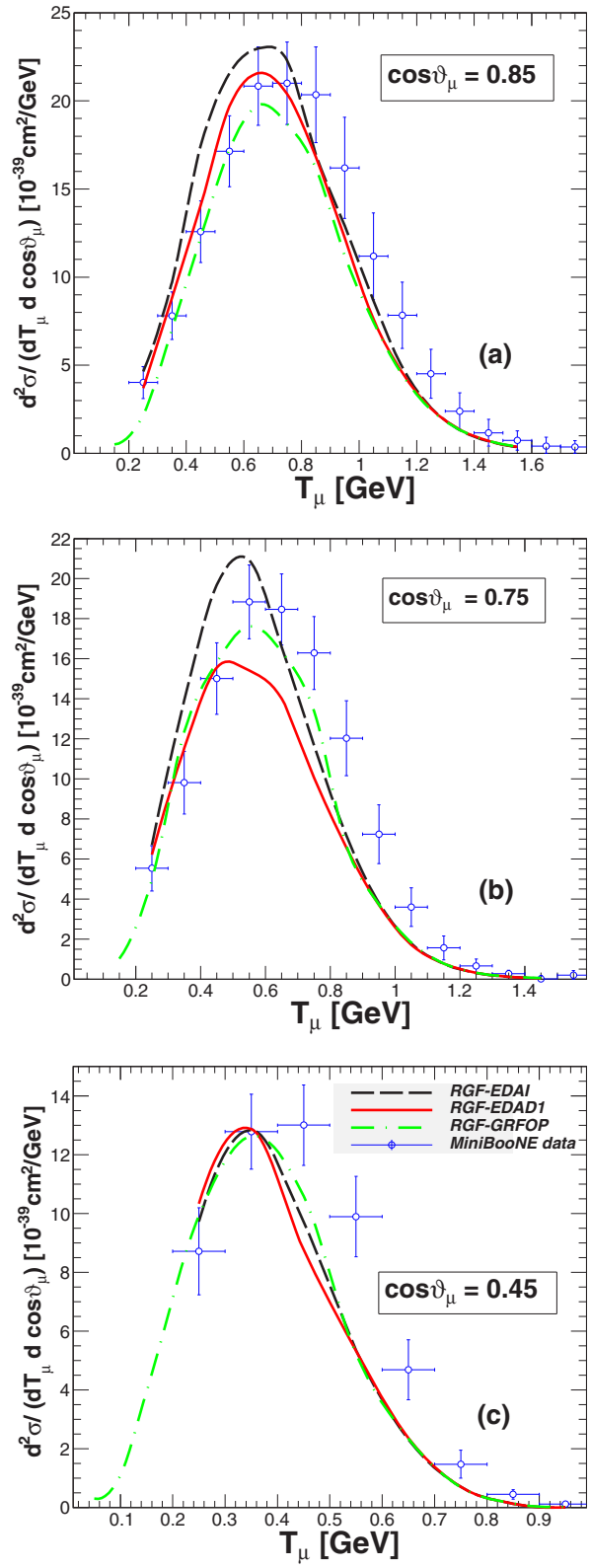

FIG. 8. Flux-averaged double-differential cross section per target nucleon for the CCQE $^{12}C(\nu_\mu,\mu^-)$ reaction as a function of the muon kinetic energy T_μ for three bins of the muon scattering angle $\cos\vartheta$ calculated with the RGF-GRFOP (dot-dashed lines), the RGF-EDAD1 (solid lines), and the RGF-EDAI (dashed lines). The experimental data are from the MiniBooNE Collaboration [57].

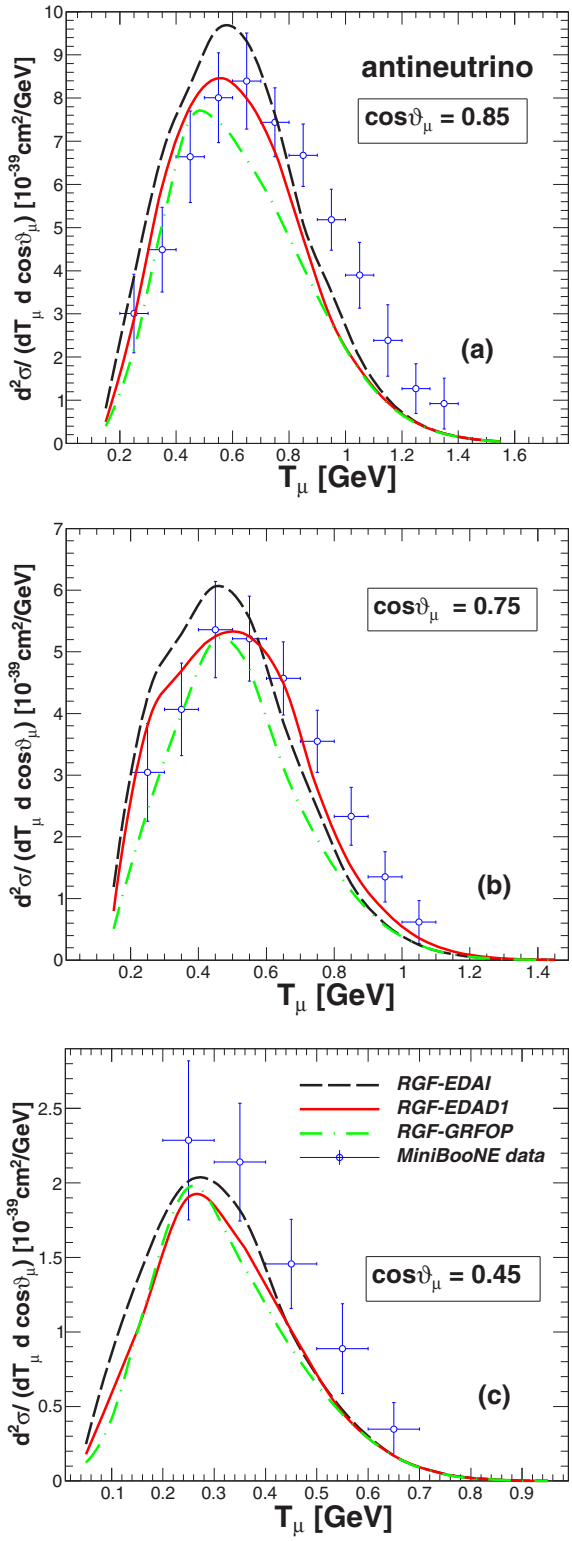

FIG. 9. The same as in Fig. 8, but for $\bar{\nu}_\mu$ scattering. The experimental data are from the MiniBooNE Collaboration [55].

calculations and satisfactorily described by the RGF-EDAD1 calculations. The RGF-GRFOP results are always smaller that the RGF-EDAI and the RGF-EDAD1 ones in panel (a) of Figs. 8 and 9, for the bin $0.8 \leqslant \cos\vartheta_\mu \leqslant 0.9$, while in panel (b) of Fig. 8, for the bin $0.7 \leqslant \cos\vartheta_\mu \leqslant 0.8$, they are larger than the RGF-EDAD1 results and in better agreement with the data. Similar results in comparison with data are produced by the three RGF calculations in panel (c) of Figs. 8 and 9, for the bin $0.4 \leqslant \cos\vartheta_\mu \leqslant 0.5$.

The differences among the RGF results with the three OPs are due to the different imaginary parts (see Fig. 5), in particular, for the energies considered in kinematics with the lowest ϑ_μ and larger T_μ. The three OPs provide in general slightly different RGF results in neutrino and antineutrino scattering: the RGF-EDAI gives a reasonable agreement with ν data but tends to overestimate $\bar{\nu}$ data, which are better reproduced by the RGF-EDAD1 and the RGF-GRFOP. These differences are related to the relative strength of the vector-axial response, which is constructive in ν scattering and destructive in $\bar{\nu}$ scattering with respect to the longitudinal and transverse ones. Moreover, we have to consider that the neutrino and antineutrino fluxes at MiniBooNE are different, even if the data have been collected in the same beamline, and the comparison between the results of ν and $\bar{\nu}$ scattering is not straightforward. In fact, because the contributions of the same kinematic regions can be different in the two cases, also the contribution of the inelasticities represented in the OP and recovered by the RGF formalism can be different in ν and $\bar{\nu}$ scattering. In any case, it seems that the vector-axial response computed for the RGF-GRFOP is smaller than with the other OPs.

The total CCQE cross sections per nucleon are displayed in Fig. 10 as a function of the neutrino and antineutrino energies, E_ν and $E_{\bar{\nu}}$, and compared with the "unfolded" experimental data. Models based on the IA, which describe the FSI by means of real potentials, usually underestimate the total CCQE MiniBooNE cross sections. Larger cross sections are obtained with the RGF. In this case the differences among the RGF-EDAI, RGF-EDAD1, and RGF-GRFOP results are larger than in the differential cross sections: the RGF-EDAI gives a good agreement with the shape and the magnitude of the experimental cross section for neutrino scattering, but overestimates antineutrino scattering data. In contrast, the RGF-EDAD1 and RGF-GRFOP clearly underestimate neutrino data but give a reasonable agreement with antineutrino data.

The MiniBooNE Collaboration has recently reported [56,58] a measurement of the NCE flux-averaged differential neutrino and antineutrino cross section on CH_2 as a function of the four-momentum transferred squared Q^2. NCE reactions are sensitive to both isoscalar and isovector weak currents and thus can provide complementary information to CCQE processes that are sensitive to the isovector current only. Despite the fact that strange-quark contributions in the nucleon may show up through the isoscalar weak current, the MiniBooNE NCE cross section is nearly independent of strangeness, because the combined effects on protons and neutrons of CH_2 almost cancel. Nevertheless, NCE measurements can give us a different perspective in neutrino-nucleus scattering to further examine nuclear effects in the energy regime of the MiniBooNE Collaboration.

In Fig. 11 we present our calculated flux-averaged NCE cross sections as a function of Q^2, where $Q^2 = 2m_N \sum_i T_i$,

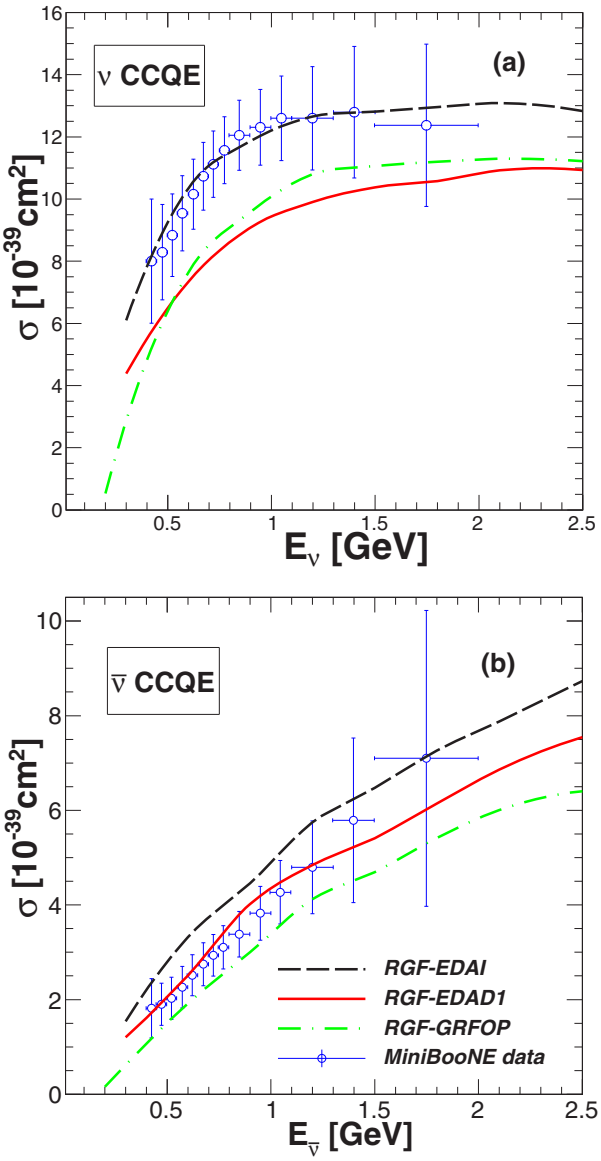

FIG. 10. Total CCQE cross section per target nucleon as a function of the neutrino energy E_ν (upper panel) and of the antineutrino energy $E_{\bar{\nu}}$ (lower panel) calculated with the RGF-GRFOP (dot-dashed lines), the RGF-EDAD1 (solid lines), and the RGF-EDAI (dashed lines). The experimental data are from the MiniBooNE Collaboration [55,57].

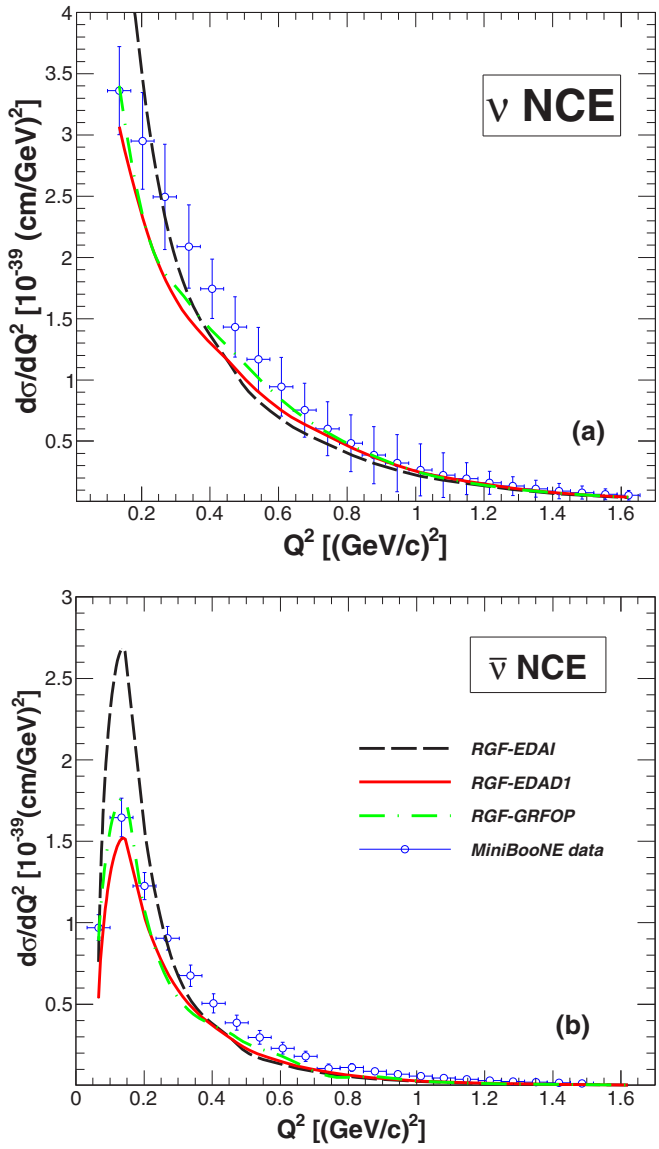

FIG. 11. Neutrino and antineutrino NCE flux-averaged cross section per target nucleon as a function of Q^2 calculated with the RGF-GRFOP (dot-dashed lines), the RGF-EDAD1 (solid lines), and the RGF-EDAI (dashed lines). The experimental data are from the MiniBooNE Collaboration [56,58].

m_N is the nucleon mass and $\sum_i T_i$ is the total kinetic energy of the outgoing nucleons. In all the NCE calculations we have adopted the standard value of the axial mass and we have neglected possible strangeness effects. In the case of neutrino scattering the RGF-EDAI results reproduce the shape and the magnitude of the experimental cross section, but overestimate the first datum at the smallest value of Q^2; the RGF-EDAD1 results underestimate the data only at the smallest values of Q^2 considered in the figure; and the RGF-GRFOP calculations generally provide a satisfactory agreement with the data. Also, in the case of antineutrino scattering the RGF results are in satisfactory agreement with the data. Close results, in the entire kinematical range of the MiniBooNE $\bar{\nu}$ flux, are obtained with RGF-EDAD1 and RGF-GRFOP, while the RGF-EDAI cross section is enhanced at $Q^2 \approx 0.1$ $(\mathrm{GeV}/c)^2$. All the RGF results are able to reasonably reproduce the first datum at $Q^2 \approx 0.06$ $(\mathrm{GeV}/c)^2$.

Ratios of cross sections, where systematic errors are largely reduced, have been proposed as alternative and useful tools to search for strangeness effects [56]. In the case of the NCE MiniBooNE cross sections, which are independent of strangeness, the antineutrino to neutrino NCE cross-section ratio, where the errors are carefully taken into account, is useful to test the predictions of different models. All the RGF calculations in Fig. 12 give, as was expected, very close results, which are practically independent of the choice of the

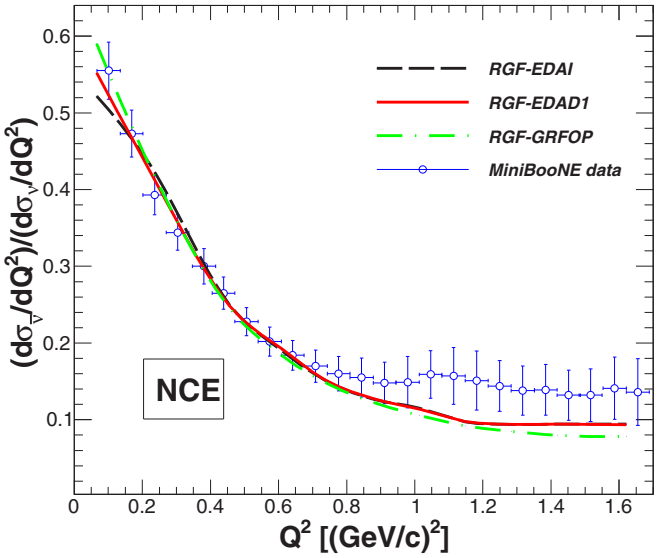

FIG. 12. Ratio of the antineutrino to neutrino NCE scattering cross section in MiniBooNE with total error. The experimental data are from the MiniBooNE Collaboration [56,58].

OP; small differences can be seen only at very low Q^2, but all the results are within the experimental errors when $Q^2 \leqslant 1$ (GeV/c)^2. Then, at higher values of Q^2, data are somewhat underestimated by the RGF results. This is because the antineutrino cross sections, in Fig. 11(b), are underestimated for large Q^2, whereas the neutrino cross sections, in Fig. 11(a), are within the error bars in the entire range of Q^2.

IV. CONCLUSION

We have obtained a new microscopic optical potential generated by folding the HLF t matrix with the relevant relativistic densities via the so-called $t\rho$ approximation. Two basic ingredients underlie the realization of these folding potentials, namely, a suitable representation for the NN interaction and an appropriate relativistic model of nuclear densities. We have extracted the vector proton density distribution from the charge distribution measured by electron scattering and we have fitted the vector neutron density to give the best χ^2 using the on-shell NN parametrization at 200 MeV, namely, the parametrization of Li *et al.* [29,30]. The corresponding scalar densities are obtained using the method given in Sec. II A [Eqs. (3) and (4)]. The same densities are used at all the energies between 20 and 1040 MeV. The GRFOP produces a very good agreement with the data for elastic scattering of protons from the ^{12}C nucleus and a value of χ^2 per degree of freedom between the EDAI and EDAD1 ones. Also, the real parts of the GRFOP are close to the EDAD1 ones, whereas the imaginary parts are lower (in absolute value) than the EDAD1 and EDAI ones. The advantage of the GRFOP is that it is, to some extent, less phenomenological, because the shapes of the potential are essentially derived from the proton and neutron densities, and these have been constrained by experimental data. The derived GRFOP fits the available elastic nucleon-nucleus data at the same level as the more phenomenological EDAI and EDAD1 potentials. In addition, we have verified that for many energies and for polarization observables, such as the analyzing power and the spin rotation parameter, the predictions of the GRFOP are in line with the ones of the EDAD1 potential.

We have tested the new GRFOP within the RGF model for QE electron scattering and (anti)neutrino-nucleus scattering at MiniBooNE kinematics. In the case of electron scattering, the RGF-GRFOP results are in generally good agreement with the magnitude and the shape of the experimental cross sections and close to the results obtained with the EDAD1 and EDAI potentials. The RGF-GRFOP results are also in good agreement with the experimental longitudinal scaling function, especially at $q = 1$ GeV/c. The RGF-GRFOP scales better than the RGF-EDAD1 and RGF-EDAI ones; this is strongly supported by the data.

In the case of CCQE (anti)neutrino scattering, the RGF-GRFOP and RGF-EDAD1 double-differential cross sections at forward angles (the cross sections at forward angles give essential contributions to the total cross sections) are lower than the RGF-EDAI ones, due to the stronger imaginary parts (as absolute value) of the EDAI potential. In contrast, for the bin $0.4 \leqslant \cos\vartheta_\mu \leqslant 0.5$ the RGF results with the three OPs are similar and all of them reproduce the data. The RGF-EDAI total cross section is in good agreement with the shape and the magnitude of the experimental data for neutrino scattering, but overestimates antineutrino scattering data. In contrast, the RGF-EDAD1 and RGF-GRFOP results clearly underestimate neutrino data but give a reasonable agreement with antineutrino data.

In the case of NCE (anti)neutrino scattering the RGF results are in satisfactory agreement with the MiniBooNE data. The main differences can be seen at $Q^2 \approx 0.1$ (GeV/c)^2, where the experimental cross section is overestimated by the RGF-EDAI, underestimated by the RGF-EDAD1, and satisfactorily described by the RGF-GRFOP.

The RGF-GRFOP results lie, in general, in between the previous RGF-EDAI and RGF-EDA1 ones and in many cases are in better agreement with the experimental data, which is very reassuring. The use of the microscopic GRFOP reduces the theoretical uncertainties in the predictions of the RGF model and confirms our previous findings: in comparison with the MiniBooNE CCQE and NCE cross sections, the RGF results are larger than the results of other models based on the impulse approximation and in better agreement with the data. The larger RGF cross sections are due to the translation to the inclusive strength of the effects of inelastic channels that are recovered in the model by the imaginary part of the OP and that are not included in other models based on the IA. Previous RGF results that showed a very large enhancement of inclusive observables are linked to a perhaps too large expression of the imaginary part of the optical potential in some imaginary fitting. Within the GRFOP, there is still a larger prediction for inclusive observables than within other IA predictions (such as PWIA, rROP, or RMF), but the difference is not as large as that found with the EDAI potential. In general, except for the figures of the unfolded total CCQE cross sections against neutrino energies, the RGF-GRFOP predictions are in similar or better agreement with the experimental data than the ones obtained with the purely phenomenological potentials.

In conclusion, our present study indicates that the RIA can provide successful Dirac optical potentials with similar fits to nucleon-nucleus elastic scattering data. In the present work the new GRFOP has been used in RGF calculations. The results shown here indicate that it can be employed as a useful alternative to phenomenological optical potentials in other nuclear reactions, for instance, in the exclusive $(e,e'p)$ reaction.

The GRFOP can be improved by extending the region of data included in the fit and, therefore, the range of validity of the parametrization. Moreover, a mass-number dependence can be included in the GRFOP parameters. An improved GRFOP would greatly increase the understanding we can gain from the comparison of RGF calculations with inclusive data. For the inclusive and the exclusive scattering and, in general, for calculations on a wide variety of nuclear reactions, which require the optical potential as a crucial and critical input, the inclusion of a mass-number dependence in the potential parameters will make the GRFOP a useful tool to study both stable and exotic nuclei.

ACKNOWLEDGMENTS

This work was partially supported by DGI (Spain) (Grant No. FPA2013-41267), by the Spanish Consolider-Ingenio 2000 program CPAN, and by the Bulgarian National Science Fund under Contracts No. DFNI-T02/19 and No. DFNI-E02/6. M.V.I. is grateful for the warm hospitality given by the UCM and for financial support during his stay there from the SiNuRSE action within the ENSAR European project.

[1] J. A. Formaggio and G. P. Zeller, Rev. Mod. Phys. **84**, 1307 (2012).
[2] J. G. Morfin, J. Nieves, and J. T. Sobczyk, Adv. High Energy Phys. **2012**, 934597 (2012).
[3] L. Alvarez-Ruso, Y. Hayato, and J. Nieves, New J. Phys. **16**, 075015 (2014).
[4] O. Benhar, P. Huber, C. Mariani, and D. Meloni, arXiv:1501.06448.
[5] F. Capuzzi, C. Giusti, and F. D. Pacati, Nucl. Phys. A **524**, 681 (1991).
[6] F. Capuzzi, C. Giusti, F. D. Pacati, and D. N. Kadrev, Ann. Phys. (NY, US) **317**, 492 (2005).
[7] A. Meucci, F. Capuzzi, C. Giusti, and F. D. Pacati, Phys. Rev. C **67**, 054601 (2003).
[8] A. Meucci, C. Giusti, and F. D. Pacati, Nucl. Phys. A **756**, 359 (2005).
[9] S. Boffi, C. Giusti, and F. D. Pacati, Phys. Rep. **226**, 1 (1993).
[10] A. Meucci, J. A. Caballero, C. Giusti, F. D. Pacati, and J. M. Udías, Phys. Rev. C **80**, 024605 (2009).
[11] A. Meucci, M. Vorabbi, C. Giusti, F. D. Pacati, and P. Finelli, Phys. Rev. C **87**, 054620 (2013).
[12] A. Meucci, M. B. Barbaro, J. A. Caballero, C. Giusti, and J. M. Udías, Phys. Rev. Lett. **107**, 172501 (2011).
[13] A. Meucci, C. Giusti, and F. D. Pacati, Nucl. Phys. A **739**, 277 (2004).
[14] A. Meucci, J. A. Caballero, C. Giusti, and J. M. Udías, Phys. Rev. C **83**, 064614 (2011).
[15] A. Meucci and C. Giusti, Phys. Rev. D **85**, 093002 (2012).
[16] A. Meucci, C. Giusti, and M. Vorabbi, Phys. Rev. D **88**, 013006 (2013).
[17] A. Meucci and C. Giusti, Phys. Rev. D **89**, 117301 (2014).
[18] A. Meucci, C. Giusti, and F. D. Pacati, Phys. Rev. D **84**, 113003 (2011).
[19] R. González-Jiménez, J. A. Caballero, A. Meucci, C. Giusti, M. B. Barbaro, M. V. Ivanov, and J. M. Udías, Phys. Rev. C **88**, 025502 (2013).
[20] A. Meucci and C. Giusti, Phys. Rev. D **89**, 057302 (2014).
[21] E. D. Cooper, S. Hama, B. C. Clark, and R. L. Mercer, Phys. Rev. C **47**, 297 (1993).
[22] E. D. Cooper, S. Hama, and B. C. Clark, Phys. Rev. C **80**, 034605 (2009).
[23] H. Wojciechowski, Int. J. Mod. Phys. E **25**, 1650008 (2016).
[24] C. J. Horowitz, Phys. Rev. C **31**, 1340 (1985).
[25] D. P. Murdock and C. J. Horowitz, Phys. Rev. C **35**, 1442 (1987).
[26] S. Hama, B. C. Clark, E. D. Cooper, H. S. Sherif, and R. L. Mercer, Phys. Rev. C **41**, 2737 (1990).
[27] O. Maxwell, Nucl. Phys. A **600**, 509 (1996).
[28] O. Maxwell, Nucl. Phys. A **638**, 747 (1998).
[29] Z. P. Li, G. C. Hillhouse, and J. Meng, Phys. Rev. C **77**, 014001 (2008).
[30] Z. P. Li, G. C. Hillhouse, and J. Meng, Phys. Rev. C **78**, 014603 (2008).
[31] C. R. Chinn, C. Elster, R. M. Thaler, and S. P. Weppner, Phys. Rev. C **51**, 1418 (1995).
[32] P. K. Deb and K. Amos, Phys. Rev. C **62**, 024605 (2000).
[33] E. J. Stephenson, R. C. Johnson, and F. Sammarruca, Phys. Rev. C **71**, 014612 (2005).
[34] H. Sakaguchi, H. Takeda, S. Toyama, M. Itoh, A. Yamagoshi, A. Tamii, M. Yosoi, H. Akimune, I. Daito, T. Inomata, T. Noro, and Y. Hosono, Phys. Rev. C **57**, 1749 (1998).
[35] J. A. Tjon and S. J. Wallace, Phys. Rev. C **32**, 1667 (1985).
[36] J. A. Tjon and S. J. Wallace, Phys. Rev. C **36**, 1085 (1987).
[37] N. Ottenstein, S. J. Wallace, and J. A. Tjon, Phys. Rev. C **38**, 2272 (1988).
[38] L. Rikus, K. Nakano, and H. V. Geramb, Nucl. Phys. A **414**, 413 (1984).
[39] L. Rikus and H. V. Geramb, Nucl. Phys. A **426**, 496 (1984).
[40] J. Zenihiro, H. Sakaguchi, T. Murakami, M. Yosoi, Y. Yasuda, S. Terashima, Y. Iwao, H. Takeda, M. Itoh, H. P. Yoshida, and M. Uchida, Phys. Rev. C **82**, 044611 (2010).
[41] S. Terashima, H. Sakaguchi, H. Takeda, T. Ishikawa, M. Itoh, T. Kawabata, T. Murakami, M. Uchida, Y. Yasuda, M. Yosoi, J. Zenihiro, H. P. Yoshida, T. Noro, T. Ishida, S. Asaji, and T. Yonemura, Phys. Rev. C **77**, 024317 (2008).
[42] K. Amos, P. Dortmans, H. Geramb, S. Karataglidis, and J. Raynnal, in *Advances in Nuclear Physics*, edited by J. Negele and E. Vogt (Springer, New York, 2002), Vol. 25, pp. 276–536.
[43] P. K. Deb, K. Amos, and S. Karataglidis, Phys. Rev. C **62**, 037601 (2000).
[44] H. F. Arellano and H. V. von Geramb, Phys. Rev. C **66**, 024602 (2002).
[45] C. Elster, T. Cheon, E. F. Redish, and P. C. Tandy, Phys. Rev. C **41**, 814 (1990).
[46] H. F. Arellano, F. A. Brieva, W. G. Love, and K. Nakayama, Phys. Rev. C **43**, 1875 (1991).

[47] R. Xu, Z. Ma, E. N. E. van Dalen, and H. Müther, Phys. Rev. C **85**, 034613 (2012).

[48] M. Martini, M. Ericson, G. Chanfray, and J. Marteau, Phys. Rev. C **80**, 065501 (2009).

[49] M. Martini, M. Ericson, G. Chanfray, and J. Marteau, Phys. Rev. C **81**, 045502 (2010).

[50] M. Martini, M. Ericson, and G. Chanfray, Phys. Rev. C **84**, 055502 (2011).

[51] M. Martini and M. Ericson, Phys. Rev. C **87**, 065501 (2013).

[52] J. Nieves, I. R. Simo, and M. J. Vicente Vacas, Phys. Rev. C **83**, 045501 (2011).

[53] J. Nieves, I. Ruiz Simo, and M. J. Vicente Vacas, Phys. Lett. B **707**, 72 (2012).

[54] J. Nieves, I. Ruiz Simo, and M. J. Vicente Vacas, Phys. Lett. B **721**, 90 (2013).

[55] A. A. Aguilar-Arevalo *et al.* (MiniBooNE Collaboration), Phys. Rev. D **88**, 032001 (2013).

[56] A. A. Aguilar-Arevalo *et al.* (MiniBooNE Collaboration), Phys. Rev. D **82**, 092005 (2010).

[57] A. A. Aguilar-Arevalo *et al.* (MiniBooNE Collaboration), Phys. Rev. D **81**, 092005 (2010).

[58] A. A. Aguilar-Arevalo *et al.* (MiniBooNE Collaboration), Phys. Rev. D **91**, 012004 (2015).

[59] C. J. Horowitz, D. P. Murdoch, and B. D. Serot, in *Computational Nuclear Physics I: Nuclear Structure*, edited by K. Langanke, J. A. Maruhn, and S. E. Koonin (Springer-Verlag, Berlin, 1991), Chap. 7.

[60] C. Horowitz and B. D. Serot, Nucl. Phys. A **368**, 503 (1981).

[61] H. D. Vries, C. D. Jager, and C. D. Vries, At. Data Nucl. Data Tables **36**, 495 (1987).

[62] M. V. Ivanov, J. R. Vignote, R. Alvarez-Rodriguez, and J. M. Udias, in *Nuclear Theory*, edited by A. Georgieva and N. Minkov (Heron, Sofia, 2011), Vol. 30, pp. 116–125; in *Proceedings of the 30th International Workshop on Nuclear Theory* (Rila Mountains, Bulgaria, 2011).

[63] M. Sharma, M. Nagarajan, and P. Ring, Phys. Lett. B **312**, 377 (1993).

[64] M. M. Sharma, G. A. Lalazissis, W. Hillebrandt, and P. Ring, Phys. Rev. Lett. **72**, 1431 (1994).

[65] S. Terashima, Systematic study of neutron density distributions of Sn isotopes by proton elastic scattering, Ph.D. thesis, Kyoto University, 2008.

[66] M. Ieiri, H. Sakaguchi, M. Nakamura, H. Sakamoto, H. Ogawa, M. Yosol, T. Ichihara, N. Isshiki, Y. Takeuchi, H. Togawa, T. Tsutsumi, S. Hirata, T. Nakano, S. Kobayashi, T. Noro, and H. Ikegami, Nucl. Instrum. Methods Phys. Res., Sect. A **257**, 253 (1987).

[67] H. O. Meyer, P. Schwandt, W. W. Jacobs, and J. R. Hall, Phys. Rev. C **27**, 459 (1983).

[68] H. O. Meyer, P. Schwandt, G. L. Moake, and P. P. Singh, Phys. Rev. C **23**, 616 (1981).

[69] H. O. Meyer, P. Schwandt, R. Abegg, C. A. Miller, K. P. Jackson, S. Yen, G. Gaillard, M. Hugi, R. Helmer, D. Frekers, and A. Saxena, Phys. Rev. C **37**, 544 (1988).

[70] A. Okamoto, T. Yamagata, H. Akimune, M. Fujiwara, K. Fushimi, M. B. Greenfield, K. Hara, K. Y. Hara, H. Hashimoto, R. Hayami, K. Kawase, M. Kinoshita, K. Nakanishi, S. Nakayama, M. Tanaka, H. Utsunomiya, N. Warashina, and M. Yosoi, Phys. Rev. C **81**, 054604 (2010).

[71] K. W. Jones, Elastic and inelastic scattering of polarized protons from carbon-12 at 400, 600, and 700 MeV, Ph.D. thesis, Los Alamos National Laboratory, 1984.

[72] G. W. Hoffmann, M. L. Barlett, D. Ciskowski, G. Pauletta, M. Purcell, L. Ray, J. F. Amann, J. J. Jarmer, K. W. Jones, S. Penttilä, N. Tanaka, M. M. Gazzaly, J. R. Comfort, B. C. Clark, and S. Hama, Phys. Rev. C **41**, 1651 (1990).

[73] G. S. Blanpied, G. W. Hoffmann, M. L. Barlett, J. A. McGill, S. J. Greene, L. Ray, O. B. Van Dyck, J. Amann, and H. A. Thiessen, Phys. Rev. C **23**, 2599 (1981).

[74] L. Ray, G. W. Hoffmann, G. S. Blanpied, W. R. Coker, and R. P. Liljestrand, Phys. Rev. C **18**, 1756 (1978).

[75] R. Bertini, R. Beurtey, F. Brochard, G. Bruge, H. Catz, A. Chaumeaux, J. Durand, J. Faivre, J. Fontaine, D. Garreta, C. Gustafsson, D. Hendrie, F. Hibou, D. Legrand, J. Saudinos, and J. Thiron, Phys. Lett. B **45**, 119 (1973).

[76] I. Sick and J. McCarthy, Nucl. Phys. A **150**, 631 (1970).

[77] W. Reuter, G. Fricke, K. Merle, and H. Miska, Phys. Rev. C **26**, 806 (1982).

[78] International Network of Nuclear Reaction Data Centres (NRDC), compilation of experimental nuclear reaction data (EXFOR/CSISRS), http://www-nds.iaea.org/exfor/exfor.htm and http://www.nndc.bnl.gov/exfor/exfor.htm.

[79] S. Boffi, C. Giusti, F. D. Pacati, and M. Radici, *Electromagnetic Response of Atomic Nuclei*, Oxford Studies in Nuclear Physics, Vol. 20 (Clarendon, Oxford, 1996).

[80] J. M. Udías, P. Sarriguren, E. Moya de Guerra, E. Garrido, and J. A. Caballero, Phys. Rev. C **48**, 2731 (1993).

[81] A. Meucci, C. Giusti, and F. D. Pacati, Phys. Rev. C **64**, 014604 (2001).

[82] A. Meucci, C. Giusti, and F. D. Pacati, Phys. Rev. C **64**, 064615 (2001).

[83] A. Meucci, Phys. Rev. C **65**, 044601 (2002).

[84] M. Radici, A. Meucci, and W. H. Dickhoff, Eur. Phys. J. A **17**, 65 (2003).

[85] C. Giusti, A. Meucci, F. D. Pacati, G. Co', and V. De Donno, Phys. Rev. C **84**, 024615 (2011).

[86] C. Maieron, M. C. Martinez, J. A. Caballero, and J. M. Udías, Phys. Rev. C **68**, 048501 (2003).

[87] J. A. Caballero, J. E. Amaro, M. B. Barbaro, T. W. Donnelly, C. Maieron, and J. M. Udías, Phys. Rev. Lett. **95**, 252502 (2005).

[88] Y. Horikawa, F. Lenz, and N. C. Mukhopadhyay, Phys. Rev. C **22**, 1680 (1980).

[89] R. M. Sealock, K. L. Giovanetti, S. T. Thornton, Z. E. Meziani, O. A. Rondon-Aramayo, S. Auffret, J.-P. Chen, D. G. Christian, D. B. Day, J. S. McCarthy, R. C. Minehart, L. C. Dennis, K. W. Kemper, B. A. Mecking, and J. Morgenstern, Phys. Rev. Lett. **62**, 1350 (1989).

[90] P. Barreau, M. Bernheim, J. Duclos, J. Finn, Z. E. Meziani, J. Morgenstern, J. Mougey, D. Royer, B. Saghai, D. Tarnowski, S. Turck-Chieze, M. Brussel, G. P. Capitani, E. De Sanctis, S. Frullani, F. Garibaldi, D. B. Isabelle, E. Jans, I. Sick, and P. D. Zimmerman, Nucl. Phys. A **402**, 515 (1983).

[91] D. B. Day, J. S. McCarthy, Z. E. Meziani, R. Minehart, R. Sealock, S. T. Thornton, J. Jourdan, I. Sick, B. W. Filippone, R. D. McKeown, R. G. Milner, D. H. Potterveld, and Z. Szalata, Phys. Rev. C **48**, 1849 (1993).

[92] O. Benhar, D. Day, and I. Sick, Rev. Mod. Phys. **80**, 189 (2008).

[93] http://faculty.virginia.edu/qes-archive/index.html.

[94] C. Maieron, T. W. Donnelly, and I. Sick, Phys. Rev. C **65**, 025502 (2002).
[95] T. W. Donnelly and I. Sick, Phys. Rev. C **60**, 065502 (1999).
[96] T. W. Donnelly and I. Sick, Phys. Rev. Lett. **82**, 3212 (1999).
[97] M. B. Barbaro, R. Cenni, A. De Pace, T. W. Donnelly, and A. Molinari, Nucl. Phys. A **643**, 137 (1998).
[98] J. A. Caballero, Phys. Rev. C **74**, 015502 (2006).
[99] J. E. Amaro, M. B. Barbaro, J. A. Caballero, and T. W. Donnelly, Phys. Rev. C **73**, 035503 (2006).
[100] A. N. Antonov, M. V. Ivanov, M. B. Barbaro, J. A. Caballero, E. Moya de Guerra, and M. K. Gaidarov, Phys. Rev. C **75**, 064617 (2007).
[101] O. Benhar and G. Veneziano, Phys. Lett. B **702**, 433 (2011).
[102] A. M. Ankowski, Phys. Rev. C **86**, 024616 (2012).
[103] V. Bernard, L. Elouadrhiri, and U. G. Meissner, J. Phys. G **28**, R1 (2002).
[104] A. Bodek, S. Avvakumov, R. Bradford, and H. Budd, Eur. Phys. J. C **53**, 349 (2008).
[105] A. De Pace, M. Nardi, W. M. Alberico, T. Donnelly, and A. Molinari, Nucl. Phys. A **741**, 249 (2004).
[106] J. E. Amaro, M. B. Barbaro, J. A. Caballero, T. W. Donnelly, and C. F. Williamson, Phys. Lett. B **696**, 151 (2011).
[107] J. E. Amaro, M. B. Barbaro, J. A. Caballero, T. W. Donnelly, and J. M. Udías, Phys. Rev. D **84**, 033004 (2011).
[108] J. E. Amaro, M. B. Barbaro, J. A. Caballero, and T. W. Donnelly, Phys. Rev. Lett. **108**, 152501 (2012).
[109] A. Bodek, H. Budd, and M. Christy, Eur. Phys. J. C **71**, 1 (2011).
[110] T. Golan, K. M. Graczyk, C. Juszczak, and J. T. Sobczyk, Phys. Rev. C **88**, 024612 (2013).
[111] T. Leitner, O. Buss, L. Alvarez-Ruso, and U. Mosel, Phys. Rev. C **79**, 034601 (2009).
[112] T. Leitner and U. Mosel, Phys. Rev. C **81**, 064614 (2010).
[113] A. M. Ankowski and O. Benhar, Phys. Rev. C **83**, 054616 (2011).
[114] E. Fernandez Martinez and D. Meloni, Phys. Lett. B **697**, 477 (2011).